

RESEARCH ARTICLE

A Mechanistic Tumor Penetration Model to Guide Antibody Drug Conjugate Design

Christina Vasalou^{1a}, Gabriel Helmlinger^{1b}, Bruce Gomes^{*}

Advanced Quantitative Sciences, Novartis, Cambridge, MA, United States of America

^{1a} Current address: Pharmacokinetics Dynamics Metabolism, Pfizer, Cambridge, MA, United States of America

^{1b} Current address: Quantitative Clinical Pharmacology, Waltham, MA, United States of America

* bruce.gomes@novartis.com



OPEN ACCESS

Citation: Vasalou C, Helmlinger G, Gomes B (2015) A Mechanistic Tumor Penetration Model to Guide Antibody Drug Conjugate Design. PLoS ONE 10(3): e0118977. doi:10.1371/journal.pone.0118977

Academic Editor: Francesco Pappalardo, University of Catania, ITALY

Received: June 10, 2014

Accepted: January 27, 2015

Published: March 18, 2015

Copyright: © 2015 Vasalou et al. This is an open access article distributed under the terms of the [Creative Commons Attribution License](https://creativecommons.org/licenses/by/4.0/), which permits unrestricted use, distribution, and reproduction in any medium, provided the original author and source are credited.

Data Availability Statement: All relevant data are within the paper and its Supporting Information files.

Funding: The authors would like to state that Novartis Institute for Biomedical Research provided support in the form of salaries for authors CV, BG, GH, but did not have any additional role in the study design, data collection and analysis, decision to publish, or preparation of the manuscript. The specific roles of these authors are articulated in the 'author contributions' section.

Competing Interests: At the time of these analyses, all authors were Novartis employees. This does not

Abstract

Antibody drug conjugates (ADCs) represent novel anti-cancer modalities engineered to specifically target and kill tumor cells expressing corresponding antigens. Due to their large size and their complex kinetics, these therapeutic agents often face heterogeneous distributions in tumors, leading to large untargeted regions that escape therapy. We present a modeling framework which includes the systemic distribution, vascular permeability, interstitial transport, as well as binding and payload release kinetics of ADC-therapeutic agents in mouse xenografts. We focused, in particular, on receptor dynamics such as endocytic trafficking mechanisms within cancer cells, to simulate their impact on tumor mass shrinkage upon ADC administration. Our model identified undesirable tumor properties that can impair ADC tissue homogeneity, further compromising ADC success, and explored ADC design optimization scenarios to counteract upon such unfavorable intrinsic tumor tissue attributes. We further demonstrated the profound impact of cytotoxic payload release mechanisms and the role of bystander killing effects on tumor shrinkage. This model platform affords a customizable simulation environment which can aid with experimental data interpretation and the design of ADC therapeutic treatments.

Introduction

Antibody-Drug Conjugates (ADCs) are therapeutic hybrid constructs comprised of a potent cancer therapeutic molecule joined by a chemical linker to an antibody directed against a tumor surface antigen. The idea of using ADCs for the direct delivery of a cytotoxic agent to the target cells was first described in the 1980s. Recent development and commercialization of two ADCs, trastuzumab DM1 (TDM1) and brentuximab vedotin have demonstrated the practicality of this biotherapeutic modality. TDM1's clinical success in breast cancer [1, 2] and brentuximab vedotin's attainment of 35% complete and 40% partial remission in Hodgkin lymphoma [3] have heralded the beginning of a wave of clinical successes. There are currently more than 200 registered clinical trials for ADC reagents, in more than 50 diseases [4]. However, not all ADC compounds are successful. Gemtuzumab ozogamicin, (marketed as Mylotarg

alter the authors' adherence to PLOS ONE policies on sharing data and materials.

and used for the treatment of acute myelogenous leukemia) was removed from the market due to an increased risk of veno-occlusive disease, leading to liver toxicity [5]. These setbacks have highlighted the complexity of designing a successful ADC therapy.

An ADC comprises three components, each having a distinct role: a) the antibody is designed to recognize specific tumor-associated antigens, b) the linker is designed to release cytotoxic payload within the cell, and c) the payload, usually a small molecular weight cytotoxic agent, achieves killing of the cancer cell. The success of an ADC therapy relies on each of these three components. Extensive optimization of these parameters has taken place over the past decades, resulting in a library of potential linker technologies and cytotoxic molecules that can produce pharmacologically active ADCs [6]. Despite this drive to maximize ADC therapeutic potential, mechanistic processes involved in the localization and activation of ADC components, combined with multiple design parameters, may result in non-intuitive drug distribution and effects, which would be difficult to understand without the use of a more systematic mathematical model.

Previous modeling efforts have explored the distribution of various biologics modalities within tumor tissues, focusing on the competing processes of target tissue binding *versus* diffusive transport [7, 8]. More recent work has focused on the biodistribution of monoclonal antibodies in a variety of preclinical species and human using more detailed physiologically-based pharmacokinetic models [9, 10]. Shah *et al.* further used a mechanistic PK/PD model to assess ADC and payload PK in various animal species, in order to predict clinical response in cancer patients, using brentuximab vedotin as an example [11]. In the present work, and for the first time, we present a mechanism-based PK/PD model that incorporates detailed descriptions of receptor dynamics, payload internalization and release mechanisms, to describe ADC and payload penetration at the cellular level and within a solid tumor, in order to project the effect in tumor mass fluctuations. Our model, currently parameterized for a mouse xenograft with the potential of extension to human, describes the importance of key intrinsic parameters, such as antigen (receptor) expression level and endocytic kinetics, in the selection of targets for ADCs; it also shows the influence of properties of the reagents that can be selected to increase the chance of a successful compound. This work presents a generic model to evaluate ADC tumor penetration that can be further calibrated to match tumor- and ADC-specific properties.

Materials and Methods

The model components, reflective of the fundamental steps involved in tumor localization, included: 1) blood flow 2) extravasation, interstitial transport and local binding/target kinetics, as well as 3) tumor growth dynamics. The model assumed a Krogh cylinder geometry to describe drug distribution from a cylindrical blood vessel segment towards surrounding tissues.

ADC Pharmacokinetics

The blood concentration was defined as a two-compartment model with a bi-exponential decay, characteristic of antibody pharmacokinetics. Typically, the local blood concentration within the Krogh cylinder is dependent on blood velocity, intravascular permeability, and the fraction of drug not bound to blood cells. Antibodies, however, due to their large size, demonstrate limited extravasation rates and are less susceptible to changes in blood flow. Concentration differences along the length of blood vessels can therefore be disregarded [7]. Blood concentration (C_{plasma}) is described as follows: $C_{plasma} = C_{plasma,0} [A * e^{-k_a * t} + B * e^{-k_b * t}]$. $C_{plasma,0}$ is the initial plasma concentration, A and B are the fractions and k_a and k_b are the clearance rates for the alpha and beta phases, respectively. ADCs were assumed to follow typical antibody PK, characterized by an initial, rapidly declining distribution phase (alpha phase) during which

the drug transports from the plasma to surrounding tissues, followed by an elimination phase (beta phase) during which the drug gets cleared from the organism. A plasma volume of 2 ml and a weight of 20 g were assumed.

Tissue Distribution and Target Receptor Kinetics

The tissue distribution model originates from a study published by Thurber *et al.* [7]. Tissue transport was governed by diffusion, hypothesized to occur through a homogeneous tissue. Model equations included only radial drug transport. Angular coordinates were disregarded under the assumption of axisymmetric drug penetration. Axial coordinates were also ignored, as previous work has demonstrated minimal variations along the length of the capillary segment due to the slower extravasation rates of antibodies [7]. The tissue distribution model therefore reduced to a one-dimensional problem, which can be visualized as a cross-section of the Krogh cylinder (Fig. 1A). Convective forces were not included in the model; previous studies have demonstrated that lack of functional lymphatic drainage elevates interstitial pressure, thereby reducing convective transport [12–14].

ADC distribution and receptor kinetics within the tumor tissue were described by the following equations:

$$\frac{d[C]}{dt} = D \left[\frac{1}{r} \frac{\partial[C]}{\partial r} + \frac{\partial^2[C]}{\partial r^2} \right] - Rxn \tag{1}$$

$$\frac{d[T]}{dt} = Rs - Rxn - kin_T[T] + k_{eT} f_{eT} [T_e] \tag{2}$$

$$\frac{d[B]}{dt} = Rxn - kin_B[B] + k_{eB} f_{eB} [B_e] \tag{3}$$

$$\frac{d[T_e]}{dt} = kin_T[T] - k_{eT} f_{eT} [T_e] - k_{eT} (1 - f_{eT}) [T_e] \tag{4}$$

$$\frac{d[B_e]}{dt} = kin_B[B] - k_{eB} f_{eB} [B_e] - k_{eB} (1 - f_{eB}) [B_e] \tag{5}$$

Simplifying:

$$\frac{d[T_e]}{dt} = kin_T \cdot [T] - k_{eT} [T_e] \tag{6}$$

$$\frac{d[B_e]}{dt} = kin_B[B] - k_{eB}[B_e] \tag{7}$$

$$Rxn = k_{on} \frac{[C]}{\epsilon} \left[\frac{[T]}{\epsilon} \Gamma \right] - k_{off}[B] \tag{8}$$

The receptor concentration at $t = 0$ (T_{init}) was computed as:

$$T_{in} = \frac{\#Rec}{A_v V_{cell}} \tag{9}$$

Where #Rec is the number of receptors per cell, A_v the Avogadro number, and V_{cell} the volume

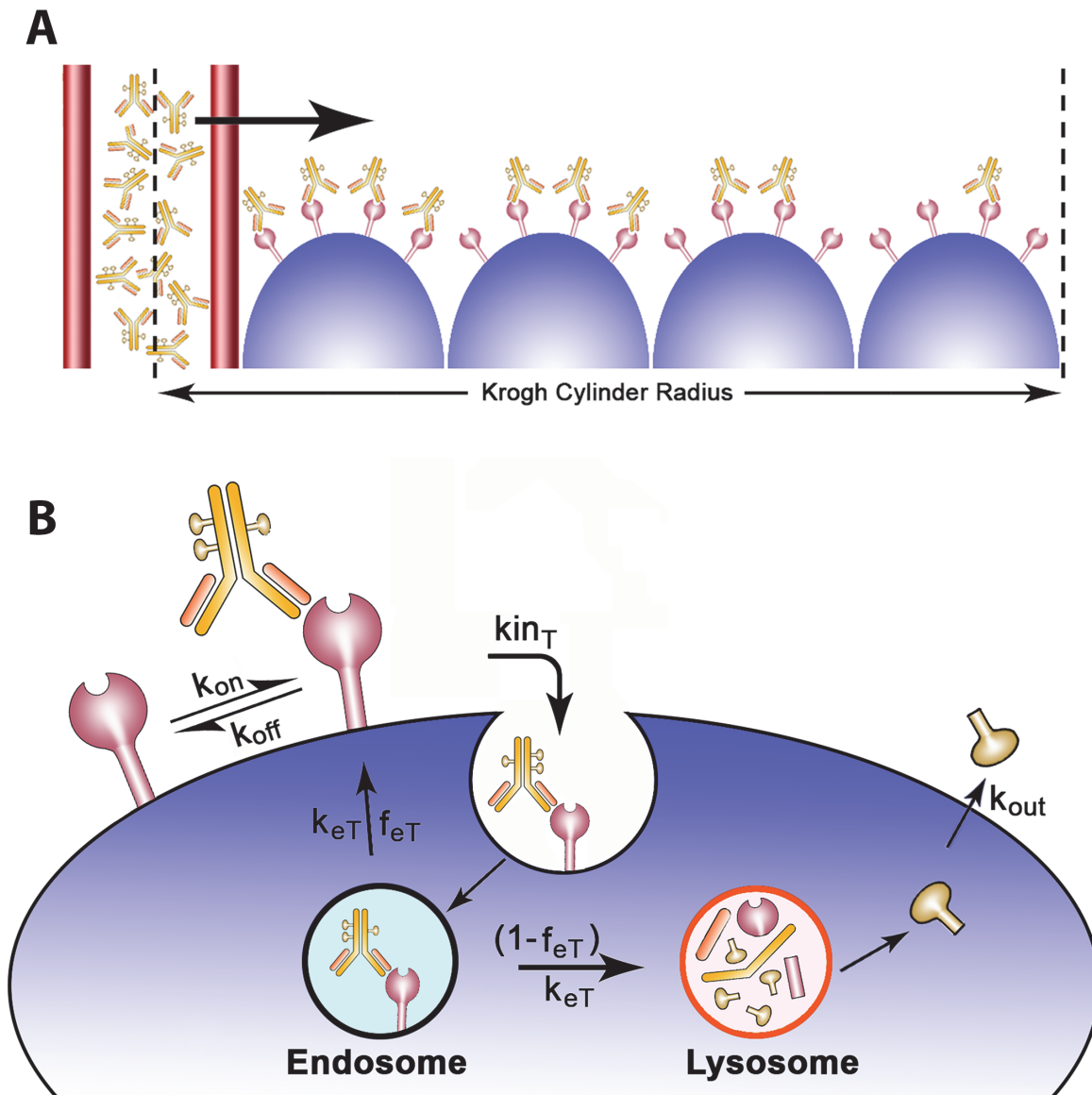


Fig 1. ADC tumor penetration schematic. A) A cross section of the Krogh cylinder illustrates the passage of ADCs through the capillary wall into the tumor tissue. The Krogh cylinder radius is equal to half the mean intercapillary distance, which is a tumor specific value. B) ADCs reversibly bind to antigen receptors located on the surface of tumor cells. Upon its formation, the ADC/receptor complex internalizes at a k_{inT} rate and is further sorted in the endosomes. The complex exits the endosomes with a k_{eT} rate and is either recycled back to the surface with a f_{eT} fraction or degraded in the lysosomes. The model assumes payload release in the lysosomes in its nominal case; upon its release, the payload can diffuse out of the cytosol with a k_{out} rate. The model assumes no payload reentry (no bystander killing effects) unless otherwise noted.

doi:10.1371/journal.pone.0118977.g001

of the cell equal to $4/3\pi(R_d)^3$, R_d being the cell radius. The model assumes target receptor localization exclusively within the tumor tissue; receptor expression in healthy tissue, followed by target mediated drug disposition, has therefore not been explored in the context of this work.

Antibody (C) was transported through the tissue with an effective diffusion coefficient D and reversibly bound the target receptor (T) with an on/off rate, k_{on} and k_{off} , respectively. Note that $k_{off} = k_{on} * K_D$, K_D being the antibody dissociation constant. Antibody (C) and target (T) tissue concentrations are restricted to the extracellular tissue volume, which results in higher interstitial *versus* overall drug concentration. This increase in concentration is accounted for by

dividing the concentration values by the void fraction (ϵ). Target concentration (T) is additionally multiplied with tumor cell mass Γ to account for the dynamic change in tumor mass, directly influencing the target receptor concentration within the Krogh cylinder.

The endocytic trafficking dynamics model, obtained from a previous study by Hendriks *et al.* [15], described the endocytic internalization of the target receptor and the competing processes of lysosomal degradation *versus* recycling back to the cell surface (Fig. 1B). Target receptors were synthesized at rate R_s , internalized at kin_T rate and exited endosomes at rate k_{eT} , with fraction f_{eT} recycling back to the surface and fraction $(1 - f_{eT})$ being degraded in the lysosomes. Antibody-receptor complexes (B) internalized at rate kin_B and were further sorted through in endosomes with an exit rate k_{eB} , a recycling fraction f_{eB} and degradation fraction $(1 - f_{eB})$. T_e and B_e describe the concentrations of the target and the antibody-target complex, respectively, within the endosome.

$$\frac{d[C_p]}{dt} = k_{eB} (1 - f_{eB}) [B_e] * DAR - k_{out} [C_p] + k_{in} \frac{[C_{p,ext}]}{\epsilon} \tag{10}$$

$$\frac{d[C_{p,ext}]}{dt} = k_{out} [C_p] - k_{in} \frac{[C_{p,ext}]}{\epsilon} + D_p \left[\frac{1}{r} \frac{\partial [C_{p,ext}]}{\partial r} + \frac{\partial^2 [C_{p,ext}]}{\partial r^2} \right] \tag{11}$$

The intracellular payload concentration C_p was released in the cytosol as a result of lysosomal degradation. We have therefore assumed non-cleavable linkers for the purpose of this model (endosomal degradation via cleavable linkers has also been explored in this study). Upon linker cleavage, the payload could further exit the cell at a k_{out} rate or reenter it at a k_{in} rate. k_{out} is a function of the retention half-life of the payload within the cell (t_p):

$$k_{out} = \frac{\ln(2)}{t_p} \tag{12}$$

Upon its exit from the cytosol to the tumor interstitial space, payload $C_{p,ext}$ diffuses with D_p at its effective diffusion coefficient. For the purpose of our simulations (and with the exception of our last figure), we assumed that the payload could not reenter tumor cells ($k_{in} = 0$, no bystander killing effect), descriptive of many commercially available payloads such as monomethyl auristatin E (MMAE).

The boundary condition at the intercapillary interface $r = R_{cap}$ defined a diffusive flux equal to the flux at the capillary wall, as driven by permeability P . Vascular permeability is an essential model parameter which determines the amount of ADC passing through the capillary wall and entering the tumor tissue. The boundary condition at $r = R_{Krogh}$ assumed no flux out of the cylinder.

$$D \frac{\partial [C]}{\partial r} \Big|_{r = R_{cap}} = P \left([C_{plasma}] - \frac{[C]}{\epsilon} \right) \tag{13}$$

$$\frac{\partial [C]}{\partial r} \Big|_{r = R_{Krogh}} = 0 \tag{14}$$

Tumor Mass Dynamics

Tumor mass dynamics equations were adjusted from Panetta *et al.* [16]. The model takes into consideration effects on the cell cycle and doubling time, as well as on the percentage of proliferating (*i.e.*, sensitive to treatment) *versus* quiescent cells. The payload concentration had a direct effect on proliferating cells, as long as the IC₅₀ value (defined as the payload concentration required to achieve a 50% reduction in cell mass at a pre-specified point in time) was exceeded.

$$\frac{dP}{dt} = (\gamma - \alpha - c_p \cdot E_{50})P + \beta Q \quad (15)$$

$$\frac{dQ}{dt} = \alpha P - \beta Q \quad (16)$$

The proliferating cell mass (P) and quiescent cell mass (Q) depended on the relative growth of cycling cells (γ)—defined as growth rate *minus* natural cell decay, the transition rate from proliferating to resting (α), the transition rate from resting to proliferating (β), and the effect of payload accumulation in the cytosol. The term E_{50} ensured payload efficacy for $C_p \geq IC_{50}$.

$$E_{50} = \frac{\frac{C_p^h}{\Gamma}}{\frac{C_p^h}{\Gamma} + IC_{50}^h} \quad (17)$$

Where h is the Hill coefficient. The payload concentration C_p was normalized by Γ to correct for fluctuations in tumor cell mass.

The parameters α and γ can be defined further by solving the following set of equations:

$$Q(t_d) + P(t_d) = 2(P(0) + Q(0)) \quad (18)$$

$$\frac{P}{Q} = r_t \quad (19)$$

Where t_d is the doubling time and r_t the proliferating-to-quiescent cell mass ratio.

Solving the equations yields:

$$\gamma = \frac{\ln(2)}{t_d \cdot r_t} (r_t + 1) \quad (20)$$

$$\alpha = \frac{\ln(2)}{t_d \cdot r_t} + \frac{\beta}{r_t} \quad (21)$$

$$\Gamma = P + Q \quad (22)$$

The tumor cell mass, Γ , was obtained by the addition of proliferating and quiescent cell masses. Γ at time zero was set equal to unity (the sum of proliferating and quiescent fractions). This mathematical manipulation enables the expression of tumor mass (Γ) for $t > 0$ as a percent change from its initial value at time zero. As a reminder, the precise tumor size is not a required input to the model since we are using Krogh cylinder geometry. Tumor mass reduction is therefore normalized to its starting value.

All model parameters and relevant references can be found in Table 1. As previously mentioned, this work presents a generic tumor model and the chosen parameters reflect average values obtained from various literature reports. The model however can be calibrated to fit specific biological systems. To simulate a particular tumor type, for example, parameters such as

Table 1. Model parameters used in simulations.

Symbol	Name	Nominal Values	Notes & References
<i>A</i>	Fraction of alpha clearance	60 (40–70%)	[8, 17]
<i>B</i>	Fraction of beta clearance	40 (30–60%)	[8, 17, 18]
<i>ka</i>	Clearance rate for alpha phase	0.6 (0.2–0.6) hr ⁻¹	[8, 18]
<i>kb</i>	Clearance rate for beta phase	0.17 (0.1–0.2) day ⁻¹	[7, 8, 18, 19]
<i>R_{Krogh}</i>	Krogh cylinder radius	72 (30–200+) μm	[20–22]
<i>R_{cap}</i>	Capillary radius	8 (5–15μm)	[20, 21, 23]
<i>P</i>	Permeability	2.8 10 ⁻⁷ (1.1–5.3 10 ⁻⁷) cm/s	[24, 25]
<i>D</i>	Effective diffusivity	1.3 10 ⁻⁷ (0.5–1.9 10 ⁻⁷) cm ² /s	[8, 13, 26, 27]
<i>k_{on}</i>	Forward reaction rate	6*10 ^{^3} nM ⁻¹ min ⁻¹	[28, 29]
<i>K_D</i>	Dissociation constant	0.1 (0.001–100) nM	Ab design parameter
	Void fraction	0.24 (0.17–0.36)	[8, 30, 31]
<i>kin_T</i>	Target Receptor internalization rate	0.01 (10 ⁻⁴ –0.5) min ⁻¹	[15, 29, 32, 33]
<i>k_{eT}</i>	Target Receptor endosomal exit rate	0.03 (0.01–0.07) min ⁻¹	[15, 32]
<i>f_{eT}</i>	Target Receptor recycling fraction	0.5 (0–0.95)	Dependent on selected target receptor [15]
<i>kin_B</i>	Ab-Target complex internalization rate	0.01 (10 ⁻⁴ –0.5) min ⁻¹	[15, 29, 32, 33]
<i>k_{eB}</i>	Ab-Target complex endosomal exit rate	0.03 (0.01–0.07) min ⁻¹	[15, 32]
<i>f_{eB}</i>	Ab-Target complex recycling fraction	0.5 (0–0.95)	Dependent on selected target receptor [15]
<i>t_p</i>	Payload retention half-life	7 (16–22) hr	[34, 35]
<i>k_{in}</i>	Payload re-entry rate into cytosol	0	No bystander effect assumed
<i>DAR</i>	Drug-Antibody ratio	3	
<i>D_p</i>	Effective diffusion coefficient of payload	3.2 10 ⁻⁶ cm ² /s	[8]
	Transition rate from resting to proliferating	0.05 days	[16]
<i>t_d</i>	Doubling time	10 (5–20+) days	Dependent on xenograft [16, 36]
<i>r_t</i>	Proliferating-to-quiescent cell mass ratio	0.1 / 0.9 (0.05 / 0.95–0.4 / 0.6)	Dependent on xenograft [16, 36]
<i>IC50</i>	IC ₅₀ concentration as measured experimentally	3 (0.1–10) nM	Dependent on type of target
<i>h</i>	Hill coefficient	100	
<i>#Rec</i>	Number of receptors per cell	10 ⁵ (10 ⁴ –2 10 ⁶)	Dependent on type of target [15]
<i>R_{cell}</i>	Cell radius	8 (5–12) μm	[37–39]

doi:10.1371/journal.pone.0118977.t001

the doubling time (*t_d*), proliferating-to-quiescent cell ratio, Krogh cylinder radius (*R_{Krogh}*), number of receptors per cell (*#Rec*), would need to be appropriately adjusted. The model was solved using the method of finite differences with a discretization step of 1 μm and was simulated using Matlab (The Mathworks; Natick, MA) with the SBPOP toolbox (www.sbtoolbox2.org), which significantly decreased simulation times.

Results

Intrinsic (System) Properties

Target Receptor Properties. To determine the effect of target receptor density on payload distribution across tumor tissue, the number of receptors per cell was first varied. Decreased antigen (receptor) levels were seen to produce more uniform, deeper-into-tissue concentration profiles (Fig. 2A), in contrast to higher antigen levels producing very steep radial gradients (Fig. 2C–D). Tissue heterogeneity observed for higher target expression was attributed to the rapid binding and immobilization of ADC near its site of entry, prohibiting the diffusion of the drug further away from the blood vessel; the so-called binding site barrier effect [30].

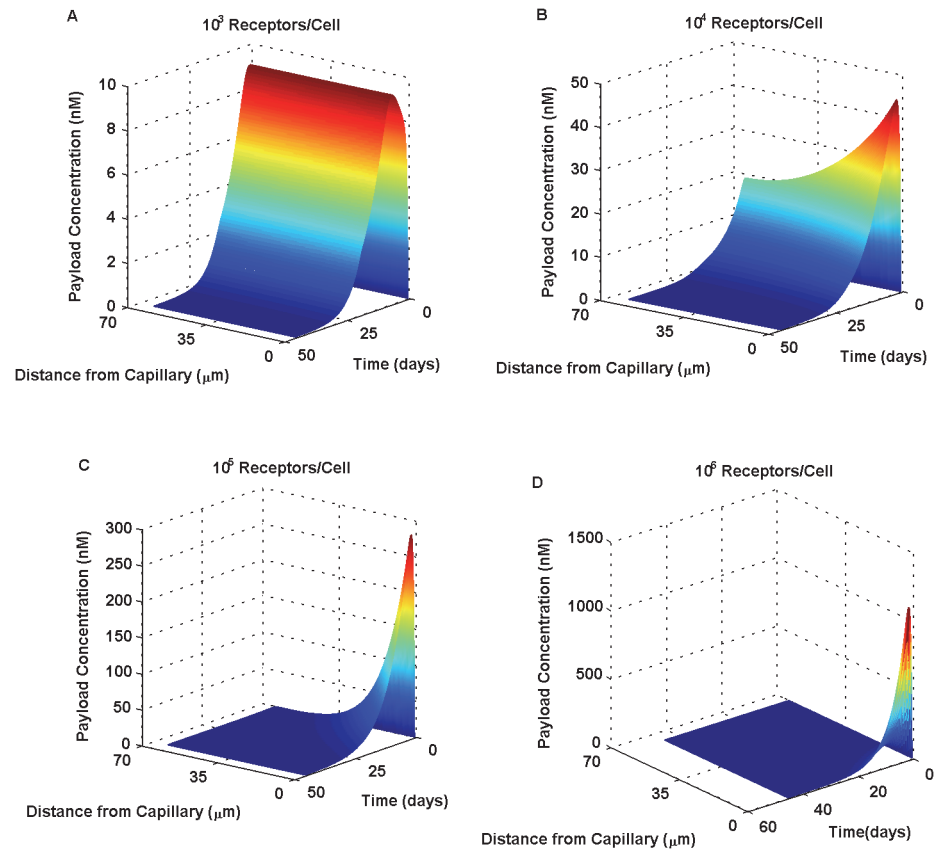


Fig 2. Increasing target receptor density has a profound effect on payload distribution across the tumor tissue. Receptors numbers per cell were varied from 10^3 (A) to 10^4 (B), 10^5 (C) and 10^6 (D). Low antigen (receptor) levels (A,B) resulted in more homogeneous payload distributions, as compared to high antigen levels (C,D) which produced pronounced, steep radial gradients. Increased receptor expression resulted in the rapid binding of ADC near its site of entry, an observation often termed as the “binding site barrier”.

doi:10.1371/journal.pone.0118977.g002

Target receptor levels were also shown to have an effect on the dynamic fluctuation of tumor mass over time (Fig. 3), as observed from the largely varied responses produced by a single intravenous administration of ADC. Tumors expressing low antigen levels were shown to reduce in mass, reaching a minimum after several days. In fact, lower receptor densities resulted in more prolonged and pronounced tumor mass reductions over time. Tumors with high receptor expression—in the order of 10^6 receptors per cell—were unable to achieve any tumor mass reduction under the particular dosing regimen tested (*i.e.*, only positive % tumor mass change values were observed).

To better visualize the effect of antigen expression on tumor mass shrinkage, we calculated the maximum tumor mass reduction *versus* the number of receptors per cell (Fig. 4). Tumors expressing lower receptor levels were easier to target and to reduce in mass, as compared to tumors expressing higher receptor levels. Increasing the number of receptors per cell above the 10^5 – 10^6 threshold resulted in the rapid impairment of ADC effect on tumor shrinkage. These results demonstrated that a decreased receptor density may, in fact, be a favorable property of the target system, implicating payload homogeneity in tumor tissues as an essential component to achieve effective ADC therapy.

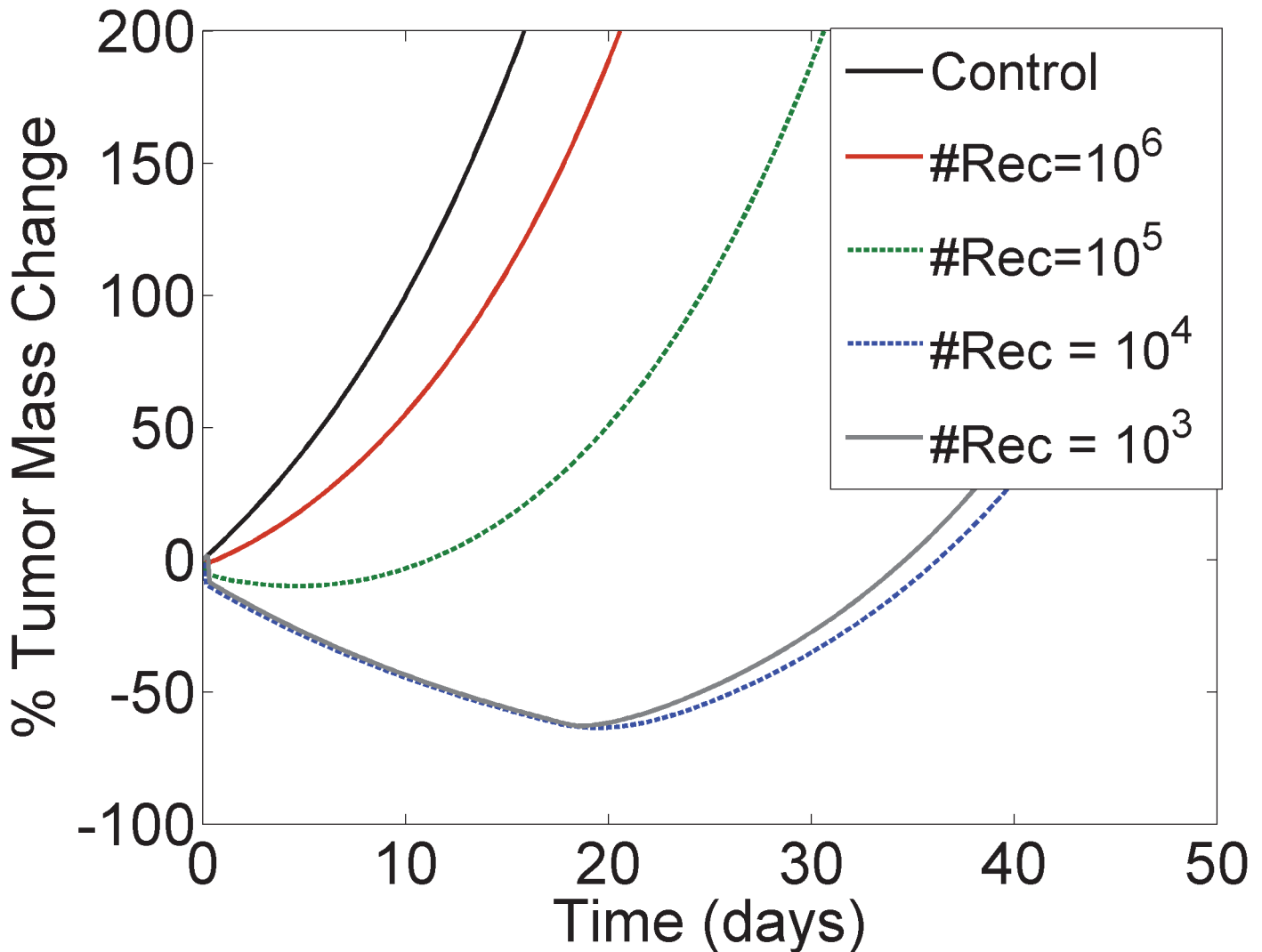


Fig 3. Tumor response to ADC therapy is driven by antigen expression levels. The Y-axis illustrates the % change in tumor mass from its initial value at time zero: negative values indicate a decrease and positive values indicate an increase in tumor mass from its baseline. Higher receptor numbers per cell ($\#Rec$) diminish the ability of the tumor to shrink in response to ADC. Control (black solid line) was compared against increasing receptor densities: $\#Rec = 10^6$ (red solid line), $\#Rec = 10^5$ (green dashed line), $\#Rec = 10^4$ (blue dashed line) and $\#Rec = 10^3$ (gray solid line). All simulations assumed a single intravenous administration of 1mg/Kg ADC, characterized by a binding affinity of $K_D = 0.1$ nM.

doi:10.1371/journal.pone.0118977.g003

Next, receptor internalization rate and recycling fraction were simultaneously varied, to investigate their combined effect on the maximum tumor mass shrinkage. Tumors expressing low receptor levels were shown to benefit from more rapid receptor internalization rates and reduced recycling fractions (Fig. 5A). By contrast, tumors with increased receptor levels were seen to benefit from slower internalization rates and higher internalization fractions (Fig. 5B). This model output is in agreement with our previous findings which demonstrated that increased receptor binding immobilizes the antibody close to its site of entry, leading to reduced antibody penetration. Increasing the recycling fraction and reducing the receptor internalization rate allow for more antibody to penetrate further away from the capillary wall, thereby improving tumor mass reduction.

Tumor Xenograft Properties. Tumor doubling time (t_d) and the proliferating-to-quiet-cent cell fraction (r_i) were next varied, to investigate their combined effect on the maximum

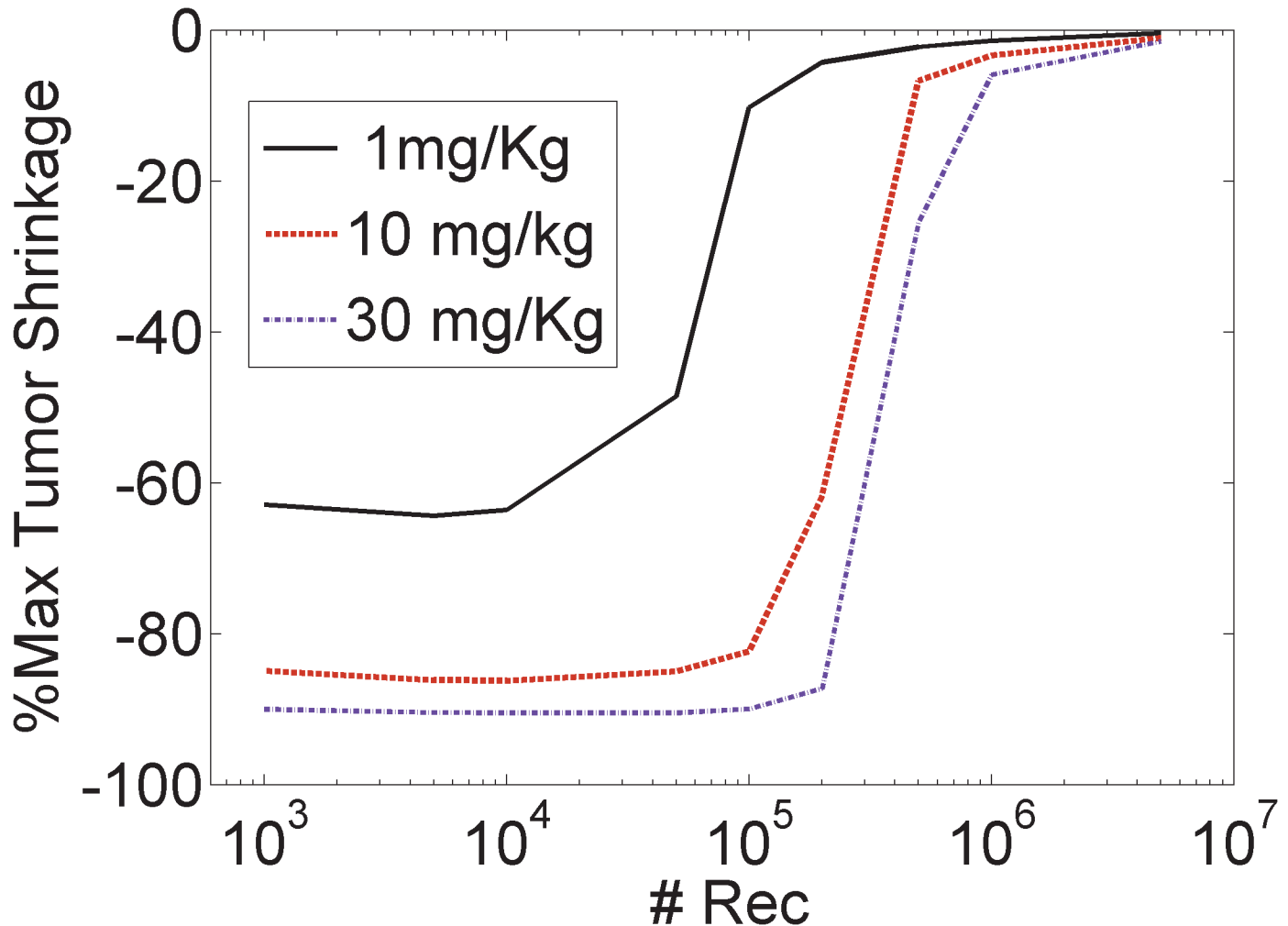


Fig 4. The maximum extent of tumor shrinkage as a function of antigen receptor levels. The Y-axis illustrates the maximal achievable tumor mass reduction; the more negative the values, the greater the tumor shrinkage, whereas a value of zero indicates that the tumor could not be shrunk. Lower receptor numbers ($\#Rec$) produced improved tumor mass loss compared to higher receptor levels. Simulations assumed a single intravenous administration of either 1 mg/Kg (black solid line), 10 mg/Kg (red dashed line) or 30 mg/Kg (purple dashed line) of ADC, characterized by a binding affinity of $K_D = 0.1$ nM.

doi:10.1371/journal.pone.0118977.g004

extent of tumor death. Note that tumor doubling time (t_d), widely used as a quantification of tumor growth rate [40], is not equivalent to the doubling time of individual proliferating cells as part of the cell cycle (defined by γ in Eq. 15). Our simulations demonstrated improved tumor shrinkage with increased tumor doubling time and increased proliferating cell fractions (Fig. 6). The proliferating-to-quiescent cell ratio was shown to have a more pronounced effect on tumor mass reduction, as compared to the tumor doubling time.

To investigate the effect of tumor vascularization on tumor mass reduction, the Krogh cylinder radius was varied—essentially, a measure of the mean intercapillary distance (Fig. 7). Reduced $RKrogh$ values produced tumors that were more accessible to the drug and therefore easier to target, as compared to less vascularized tumors characterized by high $RKrogh$ values. Our simulations demonstrated that highly vascularized tumors reduce more promptly compared to less vascularized tumors, while applying the same dosing regimen. These modeling results suggest that xenograft selection plays a key role in study endpoints, indicating the need to

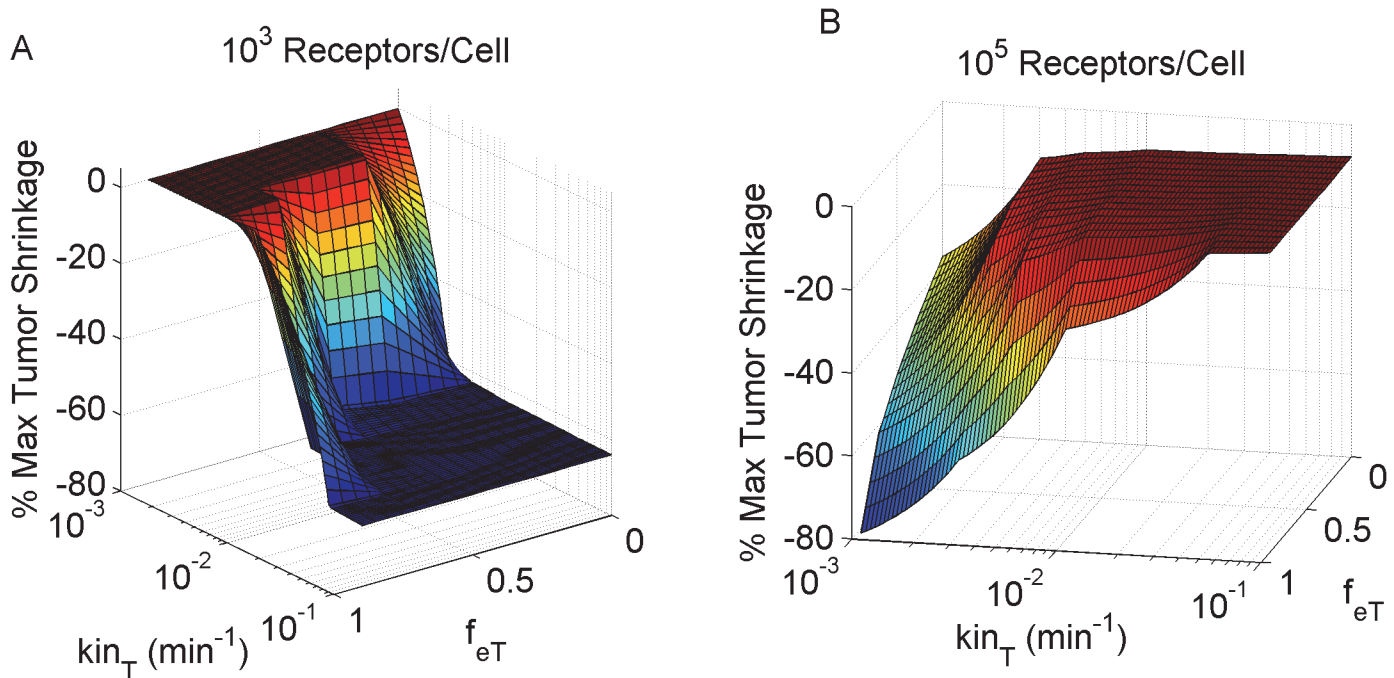


Fig 5. Tumor mass shrinkage as a function of target receptor kinetics. Increasing the internalization rate (kin_T) and reducing the receptor recycling fraction (f_{eT}) had a positive effect on tumor mass reduction, in the instance of low antigen expression levels (simulations of 10^3 receptors per cell; A). The opposite effect is noted for tumors with high antigen expression (10^5 receptors per cell B).

doi:10.1371/journal.pone.0118977.g005

interpret the success or failure of a compound in close relation to the intrinsic properties of the tumor.

Extrinsic (ADC) Properties

We next investigated the therapeutic potential of extrinsic drug properties, by varying the binding affinity and dose of administered ADC and determining their combined effect on tumors which expressed varying degrees of antigen levels (Fig. 8). Tumors expressing low antigen levels benefited, in a therapeutic sense, from low K_D values, as increasing the K_D monotonically produced inferior tumor mass shrinkage (Fig. 8A-B). By contrast, tumors with increased antigen levels exhibited an inverse response to high K_D values. In the instance of high receptor density, tumor death improved with increasing K_D and reached an asymptote after a K_D threshold value was achieved (Fig. 8C-D). As expected, higher doses of ADC produced improved tumor shrinkage for all tumor types, regardless of their antigen expression. These simulation results established a correlation between the intrinsic properties of the target tumor and the extrinsic ADC design optimization process.

To investigate the role of payload kinetics in terms of drug efficacy, scenarios of endosomal versus lysosomal payload releases were explored with the model, in addition to simulating the effect of increasing the payload retention half-life, t_p . Endosomal payload release was simulated by modifying Eq.10 as follows:

$$\frac{d[C_p]}{dt} = k_{inB} B * DAR - k_{out} [C_p] + k_{in} \frac{[C_{p,ext}]}{\epsilon} \quad (23)$$

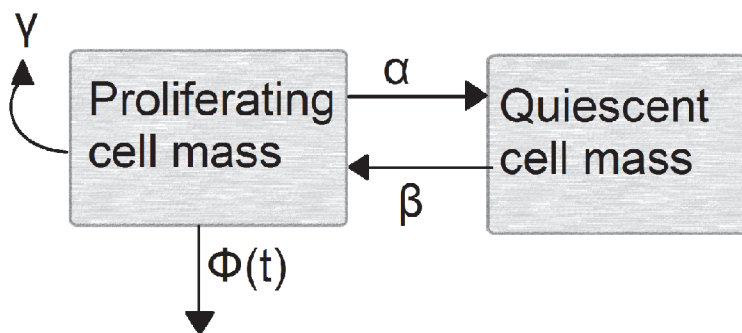
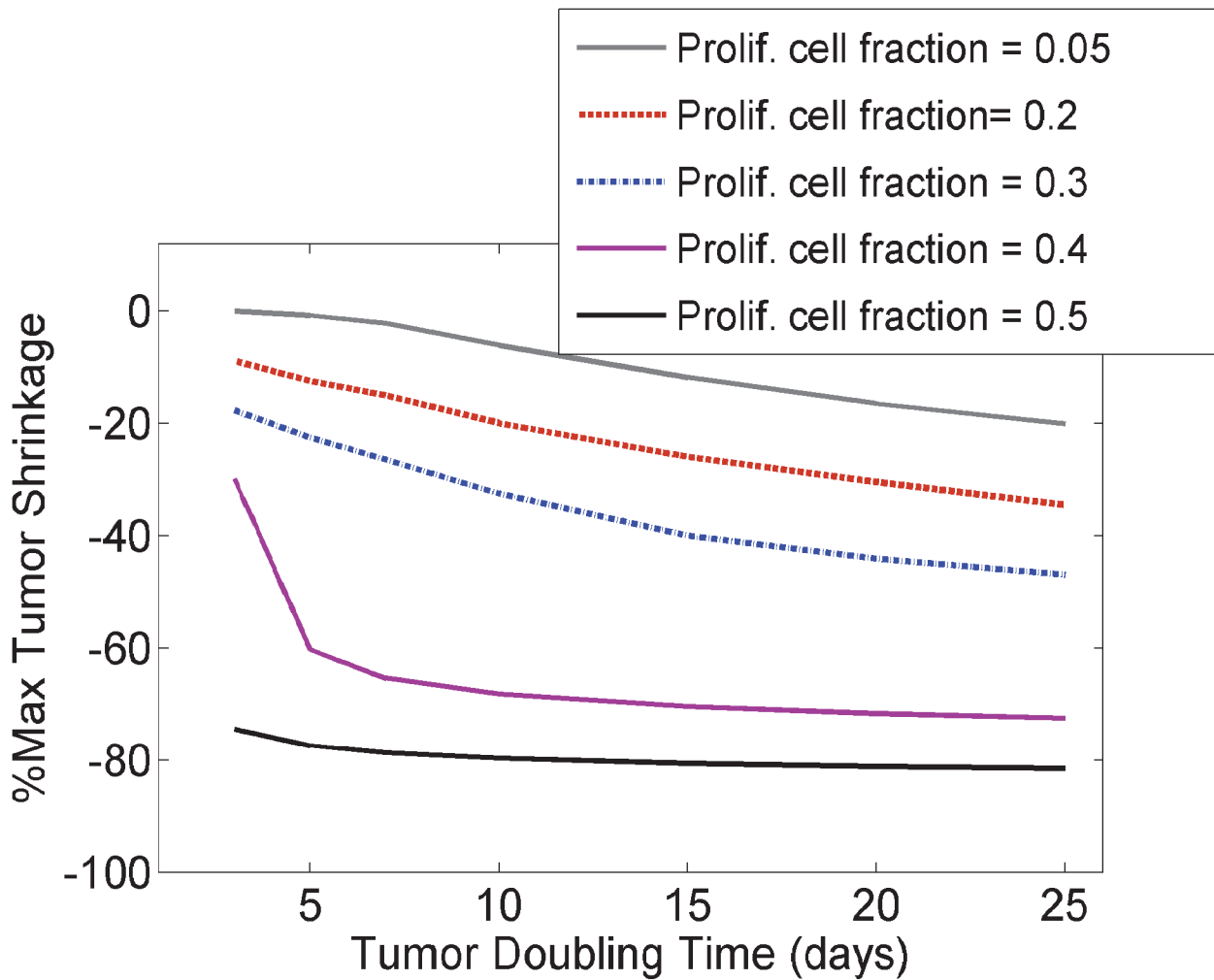


Fig 6. Intrinsic tumor growth properties affect the maximum extent of tumor shrinkage. A) Increasing tumor doubling time as well as the proliferating cell fraction enhanced tumor reduction in response to a single intravenous administration of 1mg/Kg ADC. The binding affinity was set equal to 0.1nM. Proliferating cell fractions simulated: 0.05 (gray solid line), 0.2 (red dashed line), 0.3 (blue dashed line), 0.4 (purple solid line) and 0.5 (black solid line). B) Simplified illustration of the tumor mass model, which included the dynamics of both proliferating as well as quiescent cell mass. $\Phi(t)$ indicates the proliferating mass reduction due to drug effect. More details can be found in the text.

doi:10.1371/journal.pone.0118977.g006

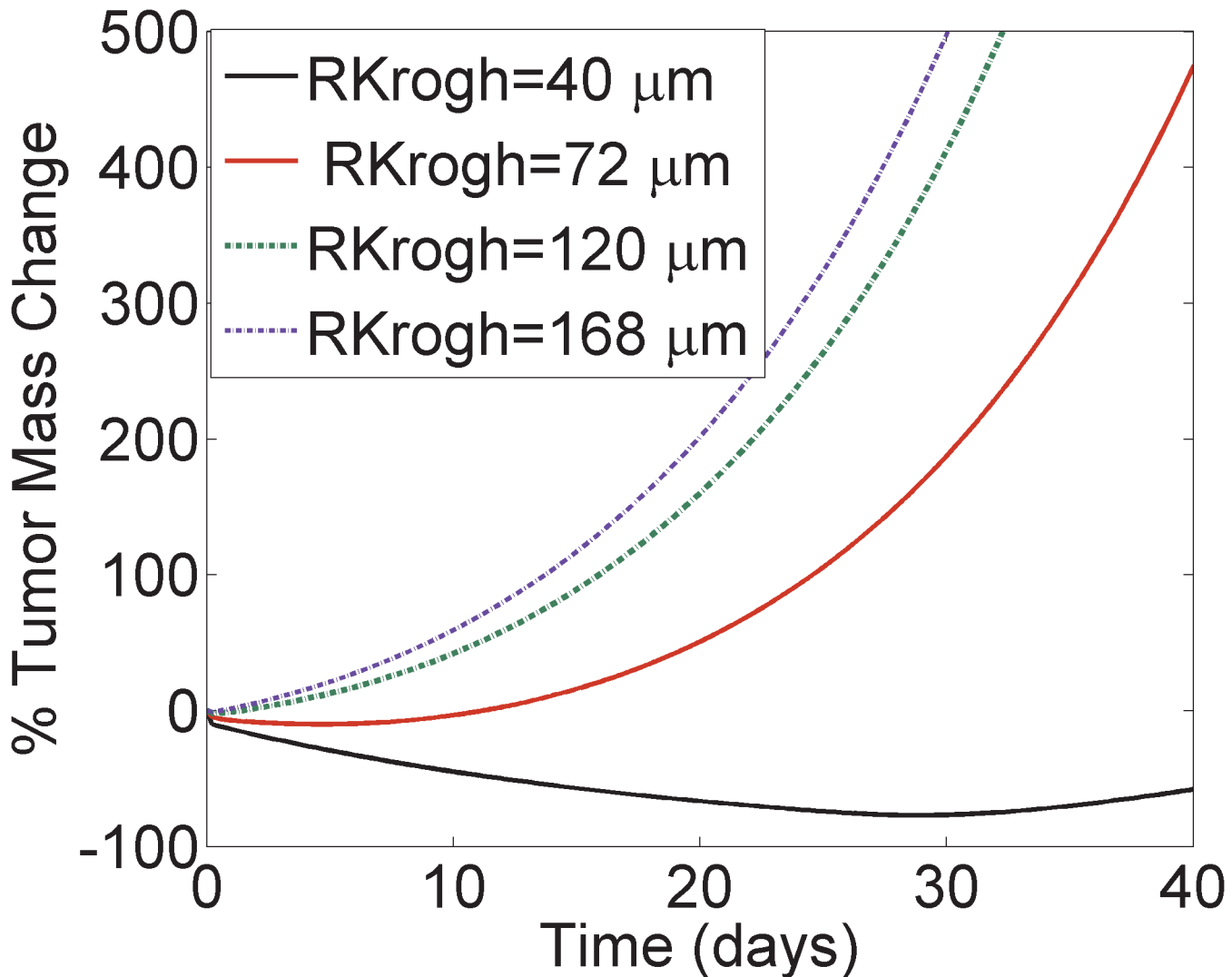


Fig 7. Tumor vascularization affects tumor response to ADC therapy. Increasing the Krogh cylinder radius ($RKrogh$) simulates tumors of decreased vascularization. $RKrogh$ was increased from $40\mu\text{m}$ (black solid line), to $72\mu\text{m}$ (red solid line), $120\mu\text{m}$ (green dashed line), and up to $168\mu\text{m}$ (purple dashed line). The graph demonstrates that highly vascularized tumors can reduce more promptly in contrast to less vascularized tumors, when applying the same ADC therapy. Dosing regimen simulated: single intravenous administration of 1mg/Kg ADC, characterized by a binding affinity of $K_D = 0.1\text{ nM}$.

doi:10.1371/journal.pone.0118977.g007

Endosomal release resulted in much higher payload concentrations in the cytosol, as compared to lysosomal cleavage (Fig. 9A-B). Additionally, a positive correlation was observed between increasing the retention half-life, indicative of the payload transfer rate from the cytosol towards the extracellular space, and the payload accumulation within the cytosol. As a consequence, tumor mass suppression was more profound in the case of endosomal *versus* lysosomal payload release, and with increasing retention half-lives (Fig. 9C).

We also addressed the question of bystander killing effect and investigated payload properties that can cause cytotoxicity to neighboring cells. For these simulations, payload re-entry into the cytosol from the local tumor environment was allowed in the model, and the ratio of transfer rates between interstitial tumor tissue and cytosol was gradually increased (k_{in}/k_{out} ; Fig. 10A). Of note, these simulations did not include the release of payload upon cell death and lysis into the interstitial space. Simulations showed that tumor cell death due to bystander

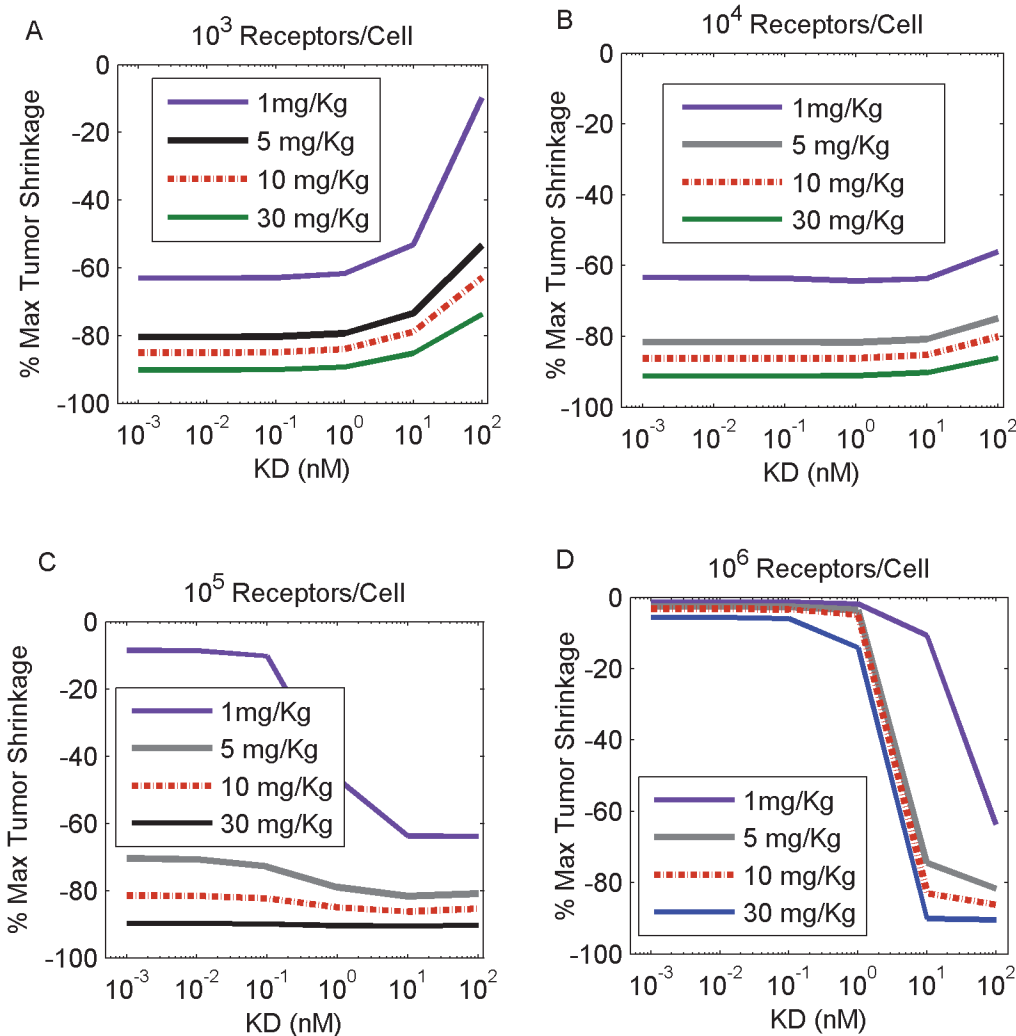


Fig 8. Increasing K_D produces a differential effect on tumor mass shrinkage, depending on antigen (receptor) level expression. Simulations included tumors that contained 10^3 (A), 10^4 (B), 10^5 (C) and 10^6 (D) receptors per cell. Increasing doses of 1mg/Kg (purple line), 5 mg/Kg (gray line), 10 mg/Kg (red dashed line) and 30 mg/kg (black line) of a single ADC intravenous administration were simulated. Our results show that decreasing K_D is beneficial when targeting tumors of low antigen expression. Contrarily, high antigen expressing tumors require increased K_D values to reduce in mass.

doi:10.1371/journal.pone.0118977.g008

effects became significant only when the payload re-entry rate (kin) became greater than the exit rate of the payload from the cytosol ($kout$). A steep decline in tumor mass was observed when $kin/kout > 1$, indicative of an onset of significant bystander killing effects (Fig. 10B).

Discussion

We developed a generalized mathematical representation of a solid tumor in a mouse model, incorporating essential mechanisms involved in ADC tumor localization and distribution. Our focus was on both intrinsic properties of the tumor itself, as well as controllable design parameters to further our understanding on effective drug delivery and ADC drug design optimization.

Our simulations demonstrated a largely varied tumor response to ADC therapy, depending on target receptor properties. It is these varied tumor responses that will guide the design of successful therapeutic agents, under conditions encountered in clinical pathology. For the

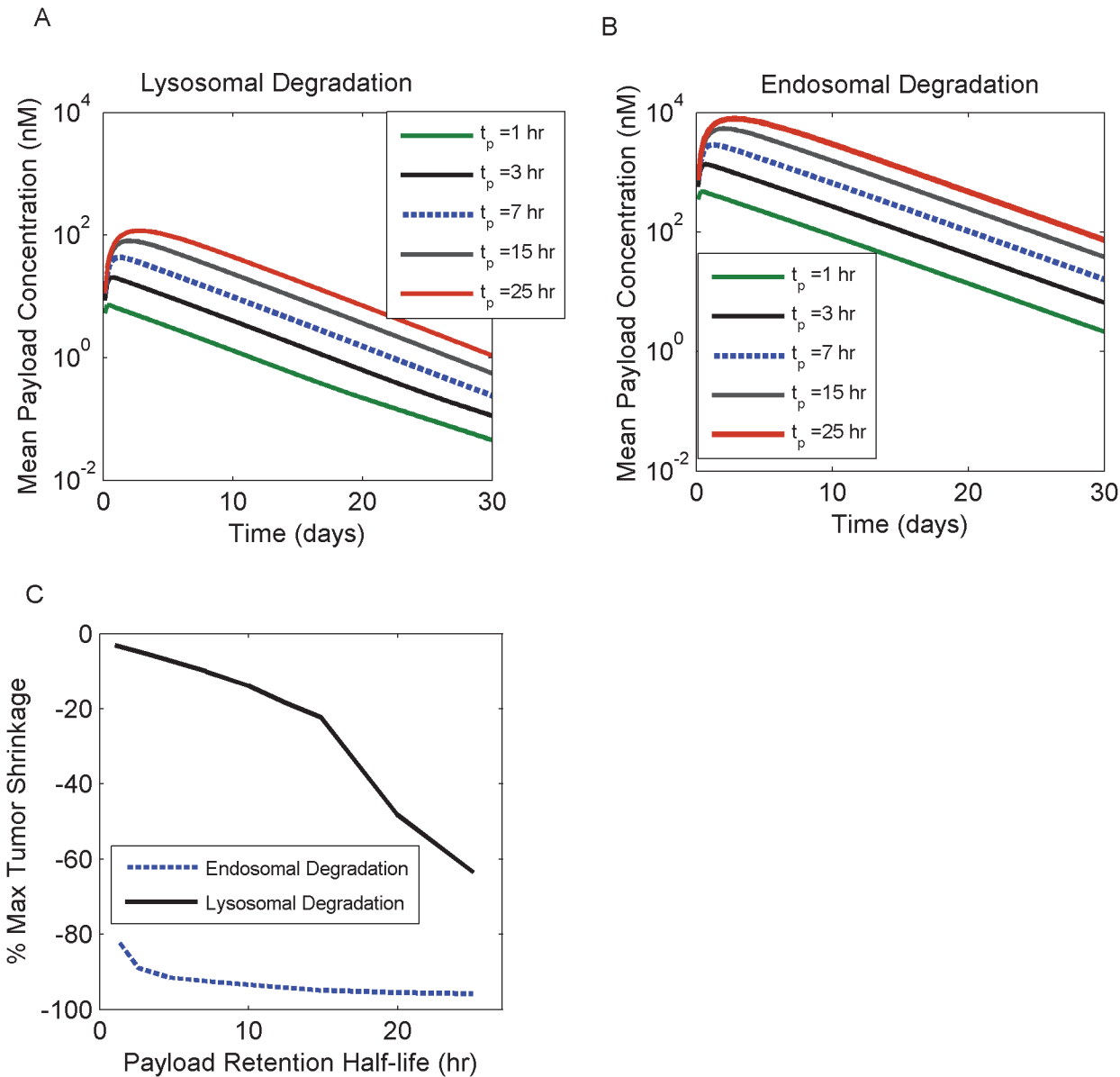


Fig 9. ADC efficacy as a function of payload cleavage mechanisms and intracellular kinetics. Lysosomal (A) versus endosomal (B) payload cleavage scenarios were simulated; the effect of payload retention half-life (t_p) was also explored, by increasing it from 1 hr (green line), to 3 hrs (gray solid line), 7 hrs (blue dashed line), 15 hrs (gray solid line), and 25 hrs (red solid line). The maximum extent of tumor shrinkage (C) was improved for endosomal (blue dashed line) versus lysosomal (black line) payload cleavage and for longer retention half-lives.

doi:10.1371/journal.pone.0118977.g009

purpose of this study, we varied receptor expression levels and endocytic trafficking dynamics. Receptor properties (such as K_D , recycling rate, internalization rate and receptor expression number) were shown to be primary drivers of payload distribution profiles across the tumor tissue: with more uniform distributions being more beneficial, in contrast to more heterogeneous, steep gradient profiles, indicative of reduced tumor penetration. Drug concentration gradients (Fig. 2 C-D) can be interpreted as a competition between local ADC/receptor binding and metabolism versus diffusion of the drug in the tissue. When diffusion is more rapid than immobilization, not-as-steep radial gradients are observed. Therefore, as target receptor expression levels increase, diffusive limitations become more prominent and cellular tissue

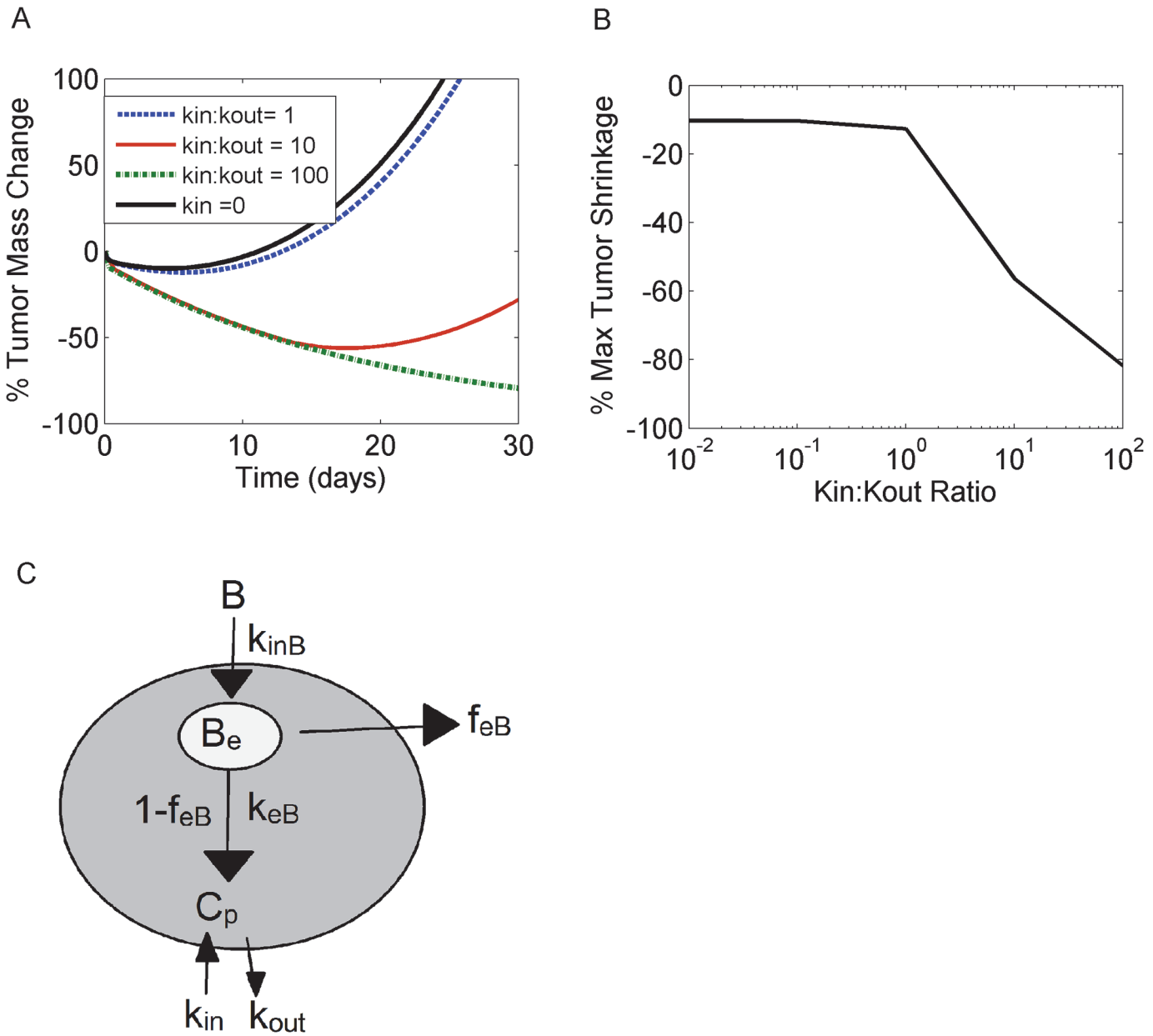


Fig 10. Bystander killing effects become significant depending on payload kinetics. Ratio of k_{in} (transfer rate from interstitial tumor tissue into the cytosol) versus k_{out} (transfer rate from the cytosol into the interstitial tumor tissue) was increased, and the effect on the % tumor mass change over time (A) and maximum tumor shrinkage (B) was reported. K_{in} with a nominal value of zero (black solid line), was gradually increased for the purpose of these simulations, to achieve k_{in} -to- k_{out} ratios equal to 1 (blue dashed line), 10 (red solid line) and 100 (green dashed line). C) Simplified illustration of ADC kinetics and payload release. Payload accumulation within the cytosol depends on k_{in} and k_{out} transfer rates. For more information on intracellular kinetic equations, refer to text.

doi:10.1371/journal.pone.0118977.g010

further away from the vessel becomes inaccessible. This concept, proposed more than 20 years ago, is termed as the “binding site barrier” [30]. Experimental studies focusing on the role of increased target density and receptor turnover rates have consistently provided growing evidence in support of this theory [41, 42].

We next focused on strategies that would be expected to increase payload tissue homogeneity, which is correlated with enhanced ADC efficacy. In particular, we investigated the role of

antibody binding affinity. Higher K_{DS} allow for a more “loose” binding state between ADC and target, enabling the drug to reach more distant targets. Similar findings have also been reported experimentally, for both antibodies as well as antibody fragments (such as single chain variable fragments, scFvs), further supporting the correlation between inefficient tumor penetration and too high affinities [43, 44]. Proper choice of antibody affinity can therefore balance unfavorable system properties such as high antigen expression, rapid internalization and turnover, which would otherwise limit the therapeutic effects of the drug. Hence the model supplies a quantitative solution to the binding site barrier dilemma.

A key design feature of ADCs is the linker connecting the cytotoxic agent to the antibody. Linker stability can influence the site and amount of payload cleavage along the intracellular trafficking pathway—with some linkers permitting the release of the cytotoxic agent in earlier endosomal compartments, bypassing the need for trafficking to the lysosomes [45, 46]. Additionally, linker cleavage produces a range of metabolites whose properties, such as size and lipophilicity, are closely associated with the chemical nature of the linker used [35]. Metabolite properties directly affect payload efflux rates from the cytosol as well as payload reentry into the cell. As a consequence linker design is a key determinant of *in vivo* efficacy [47, 48]. Payload reentry has, in fact, received increasing interest due to its implication in bystander cell killing effects and its ability to enhance ADC efficacy [47, 49]. In this work, we systematically varied payload kinetics to mimic the effects of linker selection. In our simulations, increasing payload retention half-lives were associated with improved tumor shrinkage, reflecting the impact of ADC metabolites and their kinetic properties in drug efficacy. Exploration of the competing scenarios of lysosomal *versus* endosomal payload release demonstrated superiority of the endosomal cleavage mechanism, which tends to increase the cell-killing potency of the ADC. It should be noted, however, that lysosome-independent mechanisms are characteristic of “cleavable” linkers, which are known to produce free payload or simple derivatives intracellularly, but are also less stable in circulation [46]. The advantage of endosomal cleavage is therefore tempered by lower systemic stability (*i.e.*, shorter ADC half-lives). This may reduce ADC tumor exposure and concomitantly result in toxicity in normal tissues [46]. Our model has not explored reduced ADC exposures associated with “cleavable” linkers; rather we have assumed one common PK profile regardless of the linker utilized. Finally, we looked into bystander killing effects and the conditions which allow neighboring cell cytotoxicity. Our model demonstrated that the payload uptake rate in the cancer cell needs to be higher than the payload efflux rate out of the cancer cell, in order to effectively observe bystander effects. These calculations agree with the recent modeling work on brentuximab vedotin from Shah *et al.* [11], who computed a ratio of $kin:kout = 10:1$.

This is the first example of a quantitative model that integrates key mechanistic features of tumor penetration, ADC distribution dynamics and patho-bio-physiology. This work was built on a previous model which describes vascular permeability and diffusion kinetics [7], to incorporate additional system components, such as endocytic trafficking mechanisms, payload release and tumor mass dynamics. The complete tumor penetration model allows for a thorough exploration of multiple parameter combinations leading to a better understanding of success or failure scenarios of ADC therapeutics. For instance, the model predicts reduced therapeutic effect against tumors expressing high levels of receptors, also characterized by fast internalization and low recycling fractions. But if the receptors within the same high-antigen-expressing tumor were to be internalized at slower rates, or recycled at higher fractions, a much improved therapeutic effect would be expected. Interestingly, this scenario is similar to TDM1, which targets Her2 receptors. Her2 expression reaches approximately 2×10^6 receptors per cell but also exhibits a highly increased recycling fraction of ~ 0.95 [50]. The binding site barrier effect which would be expected due to high antigen expression is therefore counteracted by the

increased recycling fraction of the receptor. Using this modeling platform, we may therefore customize simulations to address questions specific to a particular tumor type or receptor. An extension to this work would be the integration of the current running model—descriptive of the tumor dynamics—with the ADC effect in the healthy tissue, to project toxicity issues and estimate therapeutic index.

Author Contributions

Conceived and designed the experiments: CV GH BG. Analyzed the data: CV. Contributed reagents/materials/analysis tools: CV. Wrote the paper: CV GH BG.

References

1. Burris HA, Rugo HS, Vukelja SJ, Vogel CL, Borson RA, Limentani S, et al. Phase II Study of the Antibody Drug Conjugate Trastuzumab-DM1 for the Treatment of Human Epidermal Growth Factor Receptor 2 (HER2)-Positive Breast Cancer After Prior HER2-Directed Therapy. *Journal of Clinical Oncology*. 2011; 29(4):398–405. doi: [10.1200/JCO.2010.29.5865](https://doi.org/10.1200/JCO.2010.29.5865) PMID: [21172893](https://pubmed.ncbi.nlm.nih.gov/21172893/)
2. Krop I, LoRusso P, Miller KD, Modi S, Yardley D, Rodriguez G, et al. A Phase II Study of Trastuzumab-DM1 (T-DM1), a Novel HER2 Antibody-Drug Conjugate, in Patients Previously Treated with Lapatinib, Trastuzumab, and Chemotherapy. *Cancer Research*. 2009; 69(24):795S–S.
3. Younes A, Gopal AK, Smith SE, Ansell SM, Rosenblatt JD, Savage KJ, et al. Results from a pivotal phase II study of brentuximab vedotin (SGN-35) in patients with relapsed or refractory Hodgkin lymphoma (HL). *ASCO Meeting Abstracts* 2011. p. (15 suppl; abstr 8031).
4. www.clinicaltrials.gov.
5. Wadleigh M, Richardson PG, Zahrieh D, Lee SJ, Cutler C, Ho V, et al. Prior gemtuzumab ozogamicin exposure significantly increases the risk of veno-occlusive disease in patients who undergo myeloablative allogeneic stem cell transplantation. *Blood*. 2003; 102(5):1578–82. PMID: [12738663](https://pubmed.ncbi.nlm.nih.gov/12738663/)
6. Alley SC, Okeley NM, Senter PD. Antibody-drug conjugates: targeted drug delivery for cancer. *Current Opinion in Chemical Biology*. 2010; 14(4):529–37. doi: [10.1016/j.cbpa.2010.06.170](https://doi.org/10.1016/j.cbpa.2010.06.170) PMID: [20643572](https://pubmed.ncbi.nlm.nih.gov/20643572/)
7. Thurber GM, Weissleder R. A Systems Approach for Tumor Pharmacokinetics. *Plos One*. 2011; 6(9).
8. Schmidt MM, Wittrup KD. A modeling analysis of the effects of molecular size and binding affinity on tumor targeting. *Molecular Cancer Therapeutics*. 2009; 8(10):2861–71. doi: [10.1158/1535-7163.MCT-09-0195](https://doi.org/10.1158/1535-7163.MCT-09-0195) PMID: [19825804](https://pubmed.ncbi.nlm.nih.gov/19825804/)
9. Shah DK, Betts AM. Antibody biodistribution coefficients Inferring tissue concentrations of monoclonal antibodies based on the plasma concentrations in several preclinical species and human. *Mabs*. 2013; 5(2):297–305. doi: [10.4161/mabs.23684](https://doi.org/10.4161/mabs.23684) PMID: [23406896](https://pubmed.ncbi.nlm.nih.gov/23406896/)
10. Shah DK, Betts AM. Towards a platform PBPK model to characterize the plasma and tissue disposition of monoclonal antibodies in preclinical species and human. *Journal of Pharmacokinetics and Pharmacodynamics*. 2012; 39(1):67–86. doi: [10.1007/s10928-011-9232-2](https://doi.org/10.1007/s10928-011-9232-2) PMID: [22143261](https://pubmed.ncbi.nlm.nih.gov/22143261/)
11. Shah DK, Haddish-Berhane N, Betts A. Bench to bedside translation of antibody drug conjugates using a multiscale mechanistic PK/PD model: a case study with brentuximab-vedotin. *Journal of Pharmacokinetics and Pharmacodynamics*. 2012; 39(6):643–59. doi: [10.1007/s10928-012-9276-y](https://doi.org/10.1007/s10928-012-9276-y) PMID: [23151991](https://pubmed.ncbi.nlm.nih.gov/23151991/)
12. Jain RK, Baxter LT. MECHANISMS OF HETEROGENEOUS DISTRIBUTION OF MONOCLONAL-ANTIBODIES AND OTHER MACROMOLECULES IN TUMORS—SIGNIFICANCE OF ELEVATED INTERSTITIAL PRESSURE. *Cancer Research*. 1988; 48(24):7022–32. PMID: [3191477](https://pubmed.ncbi.nlm.nih.gov/3191477/)
13. Pluen A, Boucher Y, Ramanujan S, McKee TD, Gohongi T, di Tomaso E, et al. Role of tumor-host interactions in interstitial diffusion of macromolecules: Cranial vs. subcutaneous tumors. *Proceedings of the National Academy of Sciences of the United States of America*. 2001; 98(8):4628–33. PMID: [11274375](https://pubmed.ncbi.nlm.nih.gov/11274375/)
14. Baxter LT, Jain RK. TRANSPORT OF FLUID AND MACROMOLECULES IN TUMORS. 4. A MICROSCOPIC MODEL OF THE PERIVASCULAR DISTRIBUTION. *Microvascular Research*. 1991; 41(2):252–72. PMID: [2051960](https://pubmed.ncbi.nlm.nih.gov/2051960/)
15. Hendriks BS, Opresko LK, Wiley HS, Lauffenburger D. Coregulation of epidermal growth factor receptor/human epidermal growth factor receptor 2 (HER2) levels and locations: Quantitative analysis of HER2 overexpression effects. *Cancer Research*. 2003; 63(5):1130–7. PMID: [12615732](https://pubmed.ncbi.nlm.nih.gov/12615732/)
16. Panetta JC. A mathematical model of breast and ovarian cancer treated with paclitaxel. *Mathematical Biosciences*. 1997; 146(2):89–113. PMID: [9348741](https://pubmed.ncbi.nlm.nih.gov/9348741/)

17. Thurber GM, Zajic SC, Wittrup KD. Theoretic criteria for antibody penetration into solid tumors and micrometastases. *Journal of Nuclear Medicine*. 2007; 48(6):995–9. PMID: [17504872](#)
18. Lin YS, Nguyen C, Mendoza JL, Escandon E, Fei D, Meng YG, et al. Preclinical pharmacokinetics, interspecies scaling, and tissue distribution of a humanized monoclonal antibody against vascular endothelial growth factor. *Journal of Pharmacology and Experimental Therapeutics*. 1999; 288(1):371–8. PMID: [9862791](#)
19. Holliger P, Hudson PJ. Engineered antibody fragments and the rise of single domains. *Nature Biotechnology*. 2005; 23(9):1126–36. PMID: [16151406](#)
20. Less JR, Skalak TC, Sevick EM, Jain RK. MICROVASCULAR ARCHITECTURE IN A MAMMARY-CARCINOMA—BRANCHING PATTERNS AND VESSEL DIMENSIONS. *Cancer Research*. 1991; 51(1):265–73. PMID: [1988088](#)
21. Less JR, Posner MC, Skalak TC, Wolmark N, Jain RK. Geometric resistance and microvascular network architecture of human colorectal carcinoma. *Microcirculation-London*. 1997; 4(1):25–33.
22. Porschen R, Classen S, Piontek M, Borchard F. VASCULARIZATION OF CARCINOMAS OF THE ESOPHAGUS AND ITS CORRELATION WITH TUMOR PROLIFERATION. *Cancer Research*. 1994; 54(2):587–91. PMID: [8275498](#)
23. Hilmas DE, Gillette EL. MORPHOMETRIC ANALYSES OF MICROVASCULATURE OF TUMORS DURING GROWTH AND AFTER X-IRRADIATION. *Cancer*. 1974; 33(1):103–10. PMID: [4810083](#)
24. Dellian M, Yuan F, Trubetskoy VS, Torchilin VP, Jain RK. Vascular permeability in a human tumour xenograft: molecular charge dependence. *British Journal of Cancer*. 2000; 82(9):1513–8. PMID: [10789717](#)
25. Yuan F, Dellian M, Fukumura D, Leunig M, Berk DA, Torchilin VP, et al. VASCULAR-PERMEABILITY IN A HUMAN TUMOR XENOGRAFT—MOLECULAR-SIZE DEPENDENCE AND CUTOFF SIZE. *Cancer Research*. 1995; 55(17):3752–6. PMID: [7641188](#)
26. Netti PA, Berk DA, Swartz MA, Grodzinsky AJ, Jain RK. Role of extracellular matrix assembly in interstitial transport in solid tumors. *Cancer Research*. 2000; 60(9):2497–503. PMID: [10811131](#)
27. Berk DA, Yuan F, Leunig M, Jain RK. Direct in vivo measurement of targeted binding in a human tumor xenograft. *Proceedings of the National Academy of Sciences of the United States of America*. 1997; 94(5):1785–90. PMID: [9050856](#)
28. Lauffenburger DA, LJ J. *Receptors: Models for binding, Trafficking, and Signaling*. Oxford University Press, Inc.; 1993. p. 30.
29. Felder S, Lavin J, Ullrich A, Schlessinger J. KINETICS OF BINDING, ENDOCYTOSIS, AND RECYCLING OF EGF RECEPTOR MUTANTS. *Journal of Cell Biology*. 1992; 117(1):203–12. PMID: [1556153](#)
30. Fujimori K, Covell DG, Fletcher JE, Weinstein JN. MODELING ANALYSIS OF THE GLOBAL AND MICROSCOPIC DISTRIBUTION OF IMMUNOGLOBULIN-G, F(AB)², AND FAB IN TUMORS. *Cancer Research*. 1989; 49(20):5656–63. PMID: [2790783](#)
31. Wiig H, Gyenge CC, Tenstad O. The interstitial distribution of macromolecules in rat tumours is influenced by the negatively charged matrix components. *Journal of Physiology-London*. 2005; 567(2):557–67. PMID: [15994186](#)
32. Goh LK, Sorkin A. Endocytosis of Receptor Tyrosine Kinases. *Cold Spring Harbor Perspectives in Biology*. 2013; 5(5). doi: [10.1101/cshperspect.a017459](#) PMID: [23637288](#)
33. Waters CM, Oberg KC, Carpenter G, Overholser KA. RATE CONSTANTS FOR BINDING, DISSOCIATION, AND INTERNALIZATION OF EGF—EFFECT OF RECEPTOR OCCUPANCY AND LIGAND CONCENTRATION. *Biochemistry*. 1990; 29(14):3563–9. PMID: [2354152](#)
34. Okeley NM, Miyamoto JB, Zhang XQ, Sanderson RJ, Benjamin DR, Sievers EL, et al. Intracellular Activation of SGN-35, a Potent Anti-CD30 Antibody-Drug Conjugate. *Clinical Cancer Research*. 2010; 16(3):888–97. doi: [10.1158/1078-0432.CCR-09-2069](#) PMID: [20086002](#)
35. Erickson HK, Park PU, Widdison WC, Kovtun YV, Garrett LM, Hoffman K, et al. Antibody-maytansinoid conjugates are activated in targeted cancer cells by lysosomal degradation and linker-dependent intracellular processing. *Cancer Research*. 2006; 66(8):4426–33. PMID: [16618769](#)
36. Panetta JC, Schaiquevich P, Santana VM, Stewart CF. Using pharmacokinetic and pharmacodynamic modeling and simulation to evaluate importance of schedule in topotecan therapy for pediatric neuroblastoma. *Clinical Cancer Research*. 2008; 14(1):318–25. doi: [10.1158/1078-0432.CCR-07-1243](#) PMID: [18172284](#)
37. Vona G, Sabile A, Louha M, Sitruk V, Romana S, Schutze K, et al. Isolation by size of epithelial tumor cells—A new method for the immunomorphological and molecular characterization of circulating tumor cells. *American Journal of Pathology*. 2000; 156(1):57–63. PMID: [10623654](#)

38. Isobe T, Ikeda Y, Ohta H. COMPARISON OF SIZES AND SHAPES OF TUMOR-CELLS IN PLASMA-CELL LEUKEMIA AND PLASMA-CELL MYELOMA. *Blood*. 1979; 53(5):1028–30. PMID: [435639](#)
39. Stoletov K, Montel V, Lester RD, Gonias SL, Klemke R. High-resolution imaging of the dynamic tumor cell-vascular interface in transparent zebrafish. *Proceedings of the National Academy of Sciences of the United States of America*. 2007; 104(44):17406–11. PMID: [17954920](#)
40. Mehrara E, Forssell-Aronsson E, Ahlman H, Bernhardt P. Specific growth rate versus doubling time for quantitative characterization of tumor growth rate. *Cancer Research*. 2007; 67(8):3970–5. PMID: [17440113](#)
41. Juweid M, Neumann R, Paik C, Perezbacete MJ, Sato J, Vanosdol W, et al. MICROPHARMACOLOGY OF MONOCLONAL-ANTIBODIES IN SOLID TUMORS—DIRECT EXPERIMENTAL-EVIDENCE FOR A BINDING-SITE BARRIER. *Cancer Research*. 1992; 52(19):5144–53. PMID: [1327501](#)
42. Ackerman ME, Pawlowski D, Wittrup KD. Effect of antigen turnover rate and expression level on antibody penetration into tumor spheroids. *Molecular Cancer Therapeutics*. 2008; 7(7):2233–40. doi: [10.1158/1535-7163.MCT-08-0067](#) PMID: [18645032](#)
43. Adams GP, Schier R, McCall AM, Simmons HH, Horak EM, Alpaugh RK, et al. High affinity restricts the localization and tumor penetration of single-chain Fv antibody molecules. *Cancer Research*. 2001; 61(12):4750–5. PMID: [11406547](#)
44. Rudnick SI, Lou JL, Shaller CC, Tang Y, Klein-Szanto AJP, Weiner LM, et al. Influence of Affinity and Antigen Internalization on the Uptake and Penetration of Anti-HER2 Antibodies in Solid Tumors. *Cancer Research*. 2011; 71(6):2250–9. doi: [10.1158/0008-5472.CAN-10-2277](#) PMID: [21406401](#)
45. Doronina SO, Toki BE, Torgov MY, Mendelsohn BA, Cerveny CG, Chace DF, et al. Development of potent monoclonal antibody auristatin conjugates for cancer therapy. *Nature Biotechnology*. 2003; 21(7):778–84. PMID: [12778055](#)
46. Gerber HP, Koehn FE, Abraham RT. The antibody-drug conjugate: an enabling modality for natural product-based cancer therapeutics. *Natural Product Reports*. 2013; 30(5):625–39. doi: [10.1039/c3np20113a](#) PMID: [23525375](#)
47. Erickson HK, Widdison WC, Mayo MF, Whiteman K, Audette C, Wilhelm SD, et al. Tumor Delivery and In Vivo Processing of Disulfide-Linked and Thioether-Linked Antibody-Maytansinoid Conjugates. *Bioconjugate Chemistry*. 2010; 21(1):84–92. doi: [10.1021/bc900315y](#) PMID: [19891424](#)
48. Szakacs G, Paterson JK, Ludwig JA, Booth-Genthe C, Gottesman MM. Targeting multidrug resistance in cancer. *Nature Reviews Drug Discovery*. 2006; 5(3):219–34. PMID: [16518375](#)
49. Kovtun YV, Audette CA, Ye YM, Xie HS, Ruberti MF, Phinney SJ, et al. Antibody-drug conjugates designed to eradicate tumors with homogeneous and heterogeneous expression of the target antigen. *Cancer Research*. 2006; 66(6):3214–21. PMID: [16540673](#)
50. Hendriks BS, Wiley HS, Lauffenburger D. HER2-mediated effects on EGFR endosomal sorting: Analysis of biophysical mechanisms. *Biophysical Journal*. 2003; 85(4):2732–45. PMID: [14507736](#)